THE JOURNAL OF PHYSICAL CHEMISTRY B

ARTICLE

pubs.acs.org/JPCB

Iron Chelation by Polyamidoamine Dendrimers: A Second-Order Kinetic Model for Metal−Amine Complexation

Michael R. Mankbadi,[†] Mohamed A. Barakat,[§,∥] Mohamed H. Ramadan,[§] H. Lee Woodcock,[‡] and John N. Kuhn*[,†]

[†]Department of Chemical and Biomedical Engineering, and [‡]Chemistry Department, University of South Florida, 4202 East Fowler Avenue, ENB 118, Tampa, Florida 33620, United States

[§]Environmental Sciences Department, Faculty of Meteorology and Environment, King Abdulaziz University (KAU), Saudi Arabia

[∥]Central Metallurgical R&D Institute, P.O. Box 87 Helwan 11421, Cairo, Egypt

ABSTRACT: This study presents a kinetic model of the chelation of iron ions by generation 4 hydroxyl-terminated polyamidoamine (PAMAM) with ethylenediamine core (G4-OH). The coordination processes of iron ions from ferric chloride, $FeCl_3$, and ferrous bromide, $FeBr_2$, to G4-OH dendrimers were analyzed using ultraviolet−visible (UV−vis) spectroscopy, proton nuclear magnetic resonance (^{1}H NMR) spectroscopy, and liquid chromatography−mass spectrometry (LC−MS). In the visible region, a charge-transfer was observed when the dendrimer was added to a ferric chloride solution. This phenomenon is a ligand-to-metal charge-transfer (LMCT) between the free electron group of the dendrimer's internal amines and the dehalogenated iron ion that takes 2 h to complete at room temperature. Analysis of potential rate laws and diffusion effects led to a second-order kinetic model for this reaction. By measuring the rate coefficients as a function of temperature (22−37 °C), an apparent activation energy of 41.5 kJ/mol was obtained using the Arrhenius method. The results of this study will fuel research of PAMAM dendrimers for environmental, pharmaceutical, and materials applications.

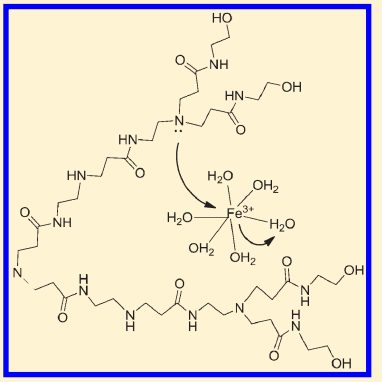

1. INTRODUCTION

Dendrimers, hyperbranched molecules composed of monomers that radiate from a central core, are emerging as an important class of polymers targeting applications in environmental remediation, nanoparticle synthesis, and nanomedicine.[1−3] Typically spherical, dendrimers are available in a range of sizes and have shown potential to serve as gene delivery agents,[4] catalytic facilitators,[5] vaccines, anticancer, antibacterial, and antiviral agents.[6] Perhaps the most popularly studied dendrimers are polyamidoamine (PAMAM) dendrimers. PAMAM dendrimers are among the least toxic dendrimers and are made from inexpensive, readily available materials.[7,8] Initial efforts in the application of PAMAM dendrimers focused on generations 1−3, which have flat ellipsoidal shapes. However, higher generation dendrimers (4 and up), which are starburst shaped, were logical extensions and are particularly appealing for modern applications.[1,9]

PAMAM dendrimers' key property is their ability to chelate metal ions from solutions. This attribute has primarily been exploited in the synthesis of metal-nanoparticles;[2,3,5,10] however, recently dendrimer-based chelation has gained interest. For example, metal-intoxication is a serious environmental concern as toxic metals are increasingly deposited into water, soil, and, inevitably, air and food. In fact, accumulation of iron, copper, and zinc in the body has been linked to neurodegenerative and psychological diseases such as Alzheimer's, Parkinson's, depression, memory loss, seizures, and dementia.[11] Additionally, a life-saving treatment for sickle-cell disease and thalassemia, the two most common hemoglobinopathies, is blood transfusion,[12,13] a treatment that has several detrimental side effects, including iron overload. Consequently, strategies to efficiently and selectively chelate heavy metal ions are an active area of research.

Current chelation therapies are limited by their (1) large, prohibitive size, (2) inability to withstand the body's acidity, (3) toxicity and the potential to deplete the body's metals to dangerously low levels, and (4) inability to get into the brain and permeate the blood−brain barrier.[8,11] PAMAM dendrimers have many attractive properties for both biological and environmental chelation. For example, studies have shown many PAMAM dendrimers to be nontoxic or only mildly toxic and likely candidates for oral administration.[6,8] Additionally, they have shown potential to surpass traditional chelating agents for removal of toxic metal ions from water[14] and to serve as fluorescent sensors.[15]

Hydroxyl and amine-terminated PAMAM dendrimers are, perhaps, the most popularly studied for metal complexation applications. PAMAM with OH terminal groups are especially nontoxic due to a lack of surface amines.[16] Encapsulation of metal ions by generation 4 hydroxyl-terminated PAMAM (G4-OH; Figure 1) involves coordinating each metal ion with one of the dendrimer's 62 tertiary amine sites.[17] Although there has been investigation of the surface properties and dynamics of PAMAM

Received: September 5, 2011
Revised: October 11, 2011
Published: October 13, 2011

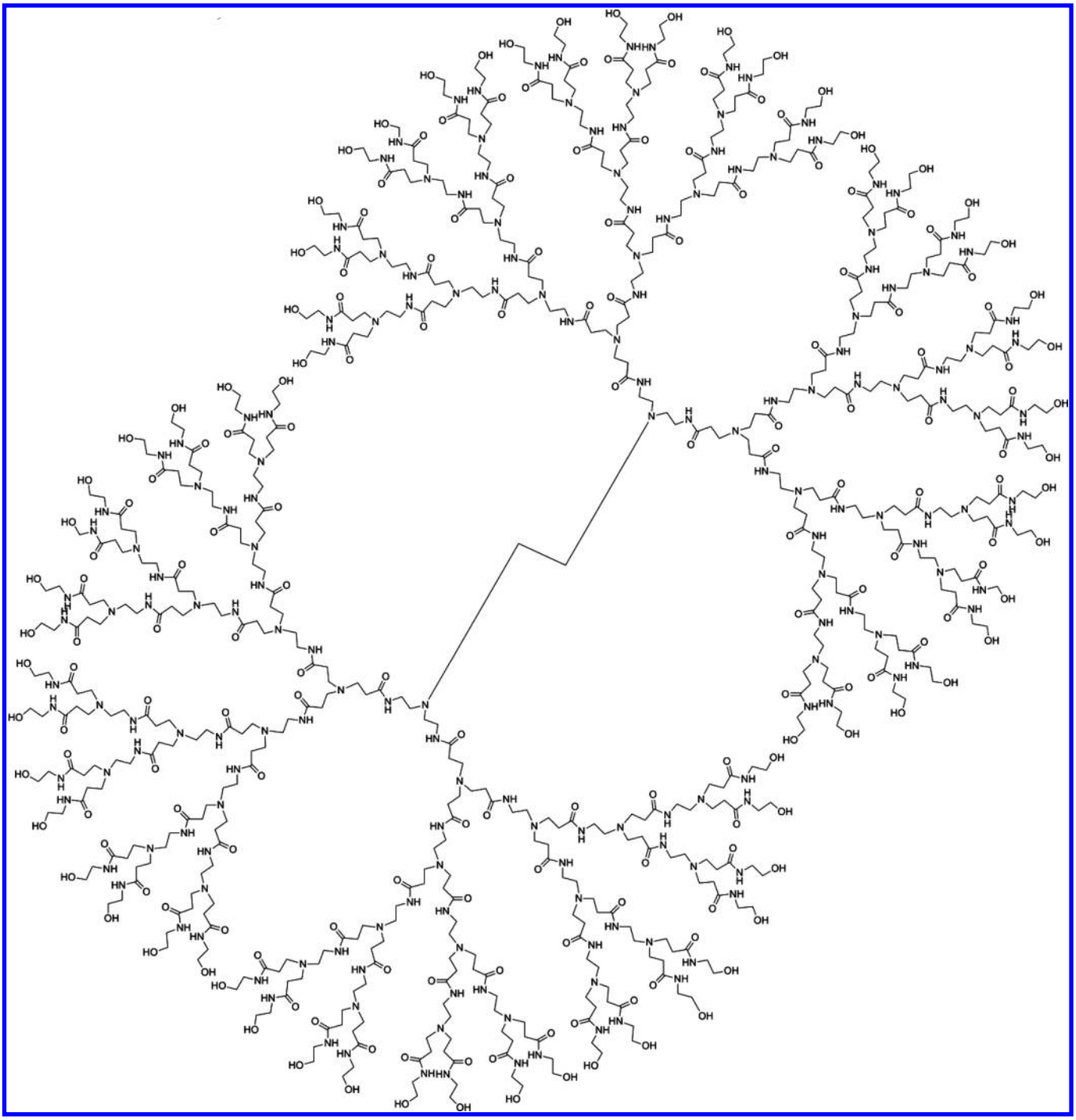

Figure 1. Generation 4 polyamidoamine with an ethylenediamine core and hydroxyl termination (referred to as G4-OH).

dendrimers, there is little information available on the metal chelation kinetics. Such information is essential for the use of PAMAM dendrimers in separation processes.

In the current work, chelation processes are kinetically modeled using transient ultraviolet−visible (UV−vis) spectroscopy data (generally involving a 40:1 Fe metal ion-to-dendrimer molecular ratio, allowing for some unsaturation of the tertiary amines). Kinetic rate constants are obtained from fitting to a second-order rate law, which was validated by analysis of other rates laws and diffusion considerations. Chelation results are confirmed by time-resolved liquid chromatography−mass spectrometry (LC−MS) and hydrogen nuclear magnetic resonance spectroscopy (^{1}H NMR). The effect of temperature on the chelation kinetics is determined by fitting the rate constants to the Arrhenius equation.

2. EXPERIMENTAL SECTION

2.1. Materials. G4-OH with ethylenediamine core was purchased from Sigma-Aldrich. Reagent grade iron III chloride, $FeCl_3$, of 97% purity (Sigma-Aldrich) was dissolved in deionized (DI) water before use. Iron II bromide, $FeBr_2$, of 98% purity

dx.doi.org/10.1021/jp208546a |J. Phys. Chem. B 2011, 115, 13534–13540

(Sigma-Aldrich) was dissolved in DI water for UV−vis spectroscopy or in 99.9% purity deuterated dimethyl sulfoxide (DMSO), $(CD_3)_2SO$ (Cambridge Isotope Laboratories, Inc.), for ^1H NMR spectroscopy. Reagent grade sodium hydroxide, NaOH (Sigma-Aldrich), was used for pH adjustments.

2.2. Ultraviolet−Visible Spectroscopy. The as-received dendrimer solution was added to 90 vol % DI water, sonicated, and used as the reference. Ferric chloride was dissolved in DI water to form a concentration of 0.5 M, having a pH of 4. Upon addition of the aqueous dendrimer solution, the pH increases to 5. This solution was added to the aqueous dendrimer solution at a 40:1 molar ratio of iron to dendrimer. UV−vis spectroscopy measurements were taken using a Nanodrop spectrophotometer, which uses approximately 2 μL per measurement. UV−vis measurements were taken at selected time intervals, during which the sample is continuously stirred at 250 rpm. This procedure was performed at 22, 27, 32, and 37 °C. A Scientific Industries Inc. Enviro Genie was used for magnetic stirring and temperature control. The absorbance is related to the concentration through the Beer−Lambert law:

$$A = \varepsilon l C \quad (1)$$

where C represents concentration, l represents path length, A represents absorbance, and ε represents molar absorptivity. The chelation process was analyzed as a second-order reaction, and rate constants were determined from a second-order rate law plot. The molar absorptivity, which is unknown, is assumed to be constant with respect to temperature. The rate constants were fit to an Arrhenius plot to determine the activation energies. Results from various wavelengths were compared to find an average and standard deviation. Follow-up experiments were performed to test the effect of each reactant on the rate by using lower reactant concentrations.

The pH of ferrous bromide was adjusted to enhance the quality of the UV−vis measurements. Sodium hydroxide was added to the aqueous ferrous bromide solution until a pH of 7 was achieved.

2.3. Nuclear Magnetic Resonance Spectroscopy. ^1H NMR spectroscopy was performed using a Bruker 250 MHz/52 MM NMR spectrometer. Methanol was removed from the dendrimer solution under vacuum, and the dendrimer was dissolved in deuterated DMSO. Because the paramagnetic nature of ferric chloride precludes its use in NMR, ferrous bromide was used. ^1H NMR measurements were taken approximately 20 min after addition of ferrous bromide and sonication. The 40:1 iron-to-dendrimer ratio was maintained.

2.4. Liquid Chromatography−Mass Spectrometry. An Agilent liquid chromatography/mass selective detector VL series with electrospray ionization (ESI) fragmentation was used. Acetonitrile and water were the mobile phase solvents. Iron solutions were added to the dendrimer solution and stirred for 80 min at 250 rpm before dilution. The 40:1 iron-to-dendrimer ratio was maintained.

3. RESULTS AND DISCUSSION

3.1. Fe−Dendrimer Coordination and Charge-Transfer. G4-OH is a clear solid, whose UV−vis spectrum exists in the ultraviolet region at low intensities. Ferric chloride has a peak in the ultraviolet region, which decreases in absorbance (Figure 2A) immediately after dendrimer addition. This absorbance decrease is accompanied by an immediate color change from a pale-yellow color to a very pronounced golden color. In the region between

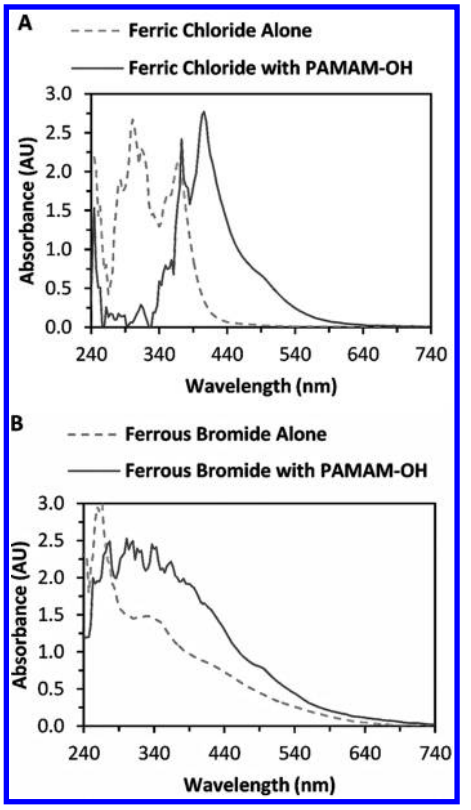

Figure 2. Full UV−vis spectrum of chelation at T = 22 °C for (A) aqueous ferric chloride before and 100 min after dendrimer addition, and (B) aqueous ferrous bromide before and 5 h after dendrimer addition.

380 and 600 nm, there is a monotonic absorbance increase lasting over 2 h at room temperature. However, most of the change is completed within the first 80 min. Researchers have observed UV−vis absorbance increases in PAMAM chelation of platinum, attributing them to ligand-to-metal charge-transfer (LMCT).[17,18] This phenomenon can be interpreted as a transfer of electrons from the HOMO of the tertiary amine to the metal center LUMO, causing the compound to adopt its unique color. The chelation rate was modeled using the progress of this LMCT band.

Dendrimer chelation of iron from ferrous bromide (Figure 2B) is somewhat longer, lasting about 8 h at room temperature. As soon as the dendrimer is added, the solution's color changes from brown to a dark-forest green. Minutes later, the color adopts a golden-brown color, comparable to that seen with ferric chloride. This rapid color change, as was similarly observed for dendrimer chelation of iron from ferric chloride, may suggest a two-stage process in which the final stable complex forms through an intermediate. The LMCT band is seen through the UV region lasting until 600 nm in the visible region. Previous studies have determined that the LMCT spectral growth is enhanced under neutral or slightly basic conditions.[17,19] The pH here was adjusted to 7 to improve solubility, allowing for cleaner UV−vis measurements.

Sun et al.[20] report that at a pH of 5, about 30% of the tertiary amines on the G4-OH are protonated. In the corresponding amine-terminated dendrimer, however, virtually all of the tertiary amines are reported to be protonated at this pH.[21,22] The tertiary amines in the hydroxyl-terminated dendrimer have a pK_a of 6.3,[23] whereas the tertiary amines within the amine-terminated dendrimer have a pK_a of 6.85.[22] Therefore, it is expected that, at the pH used

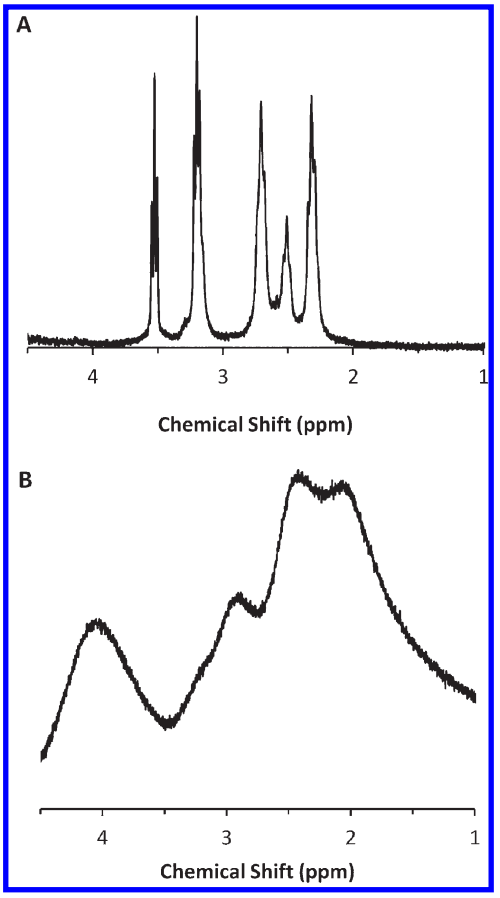

Figure 3. NMR spectra of G4-OH (A) alone and (B) after mixing with aqueous ferrous bromide for 20 min (T = 22 °C).

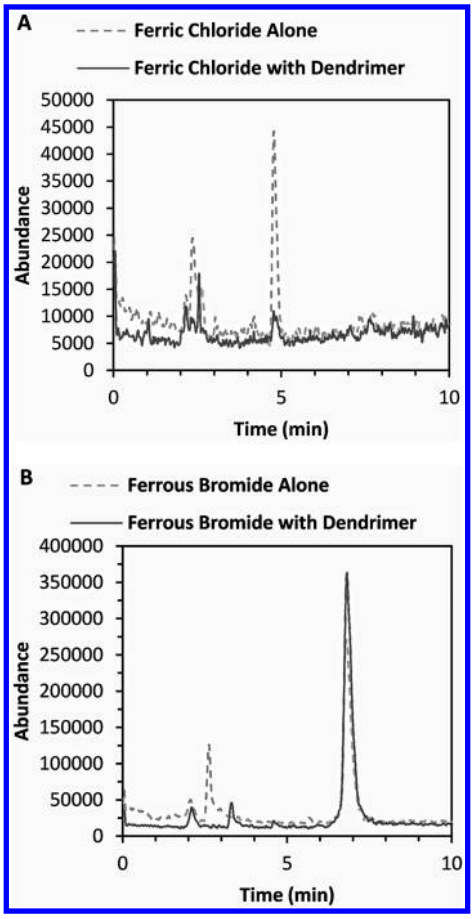

Figure 4. Liquid chromatogram of (A) aqueous ferric chloride and (B) aqueous ferrous bromide before and after the addition of the dendrimer (T = 22 °C).

for the ferric chloride experiments, coordination would be suppressed by protons at a portion of the sites. However, the increased size that results from protonation may promote coordination rates by making the structure more susceptible to solvents.[19] The inhibition from protons might also explain why the two-step color change is not seen with ferric chloride. One source[24] also suggested the possibility of amide oxygens and nitrogens assisting in the chelation. Because these groups have a pK_a different from that of the tertiary amines, their involvement in binding might also explain a longer time.

Because of the paramagnetic nature of ferric chloride, ferrous bromide was used for NMR spectroscopy (Figure 3). Several peaks, all within the region of 1 and 4 ppm, as was reported by Gomez et al.,[25] are detected. Gomez et al. assign all of the peaks to carbon-bonded hydrogens; the right-most peak (2.3 ppm) represents those closest to the amide carbon, while the left-most peak (3.5 ppm) represents those closest to the terminal hydroxyls, and the other three peaks signify those that have a neighboring nitrogen atom.[25] When ferrous bromide is added to the dendrimer, no sharp peaks can be seen. There is a broadening and flattening of the peaks, indicative of bonding between the iron and the internal amines of the dendrimer. Ooe et al.[26] had observed a similar development as a result of hydrogen bonding of the tertiary amine groups of generation 5 triethoxybenzamide (TEBA) dendrimers. In the case of Gomez et al.,[25] addition of Pd ions to G4-OH results in no peaks until reduction with BH_4^-.

Liquid chromatography reveals a major peak at about 5 min and a minor peak at 2.5 min after elution of ferric chloride (Figure 4A). The mass spectrum (Figure 5A) reveals that the major compound in both of these peaks has a molecular weight of 153.1 m/z. The expected hydrolysis reaction of the iron compounds is an acid−base exchange between the water and halogen ions.

$$FeCl_3 + 6H_2O \rightarrow Fe(OH_2)_6 + 3Cl^- \quad (2)$$

Several sources detail that as many as six oxygen groups could bind to the Fe^{3+} ion, depending on the pH.[27,28] If some hydrogen atoms had been fragmented from circulation within the mass spectrometer, it could result in a molecular weight of 153 g/mol. In the case of ferrous bromide (Figure 4B), a similar result is seen at 2.5 min after elution in the liquid chromatogram. The major compound here is 105.1 m/z (Figure 5B), again, most probably hydroxylated iron, $Fe(OH)_3$, or hydrated iron, $Fe(OH_2)_3$. This peak, as well as the two ferric chloride peaks, is reduced in size after the dendrimer is added to the solution. G4-OH has a molecular weight of 14 277 g/mol, and, therefore, it cannot be analyzed. With the system used, it is expected to take well over 10 min to elute in a liquid chromatogram.

3.2. Analysis of Diffusion Limitations. The validity of employing a kinetically limited model to the concentration profile is evaluated by first analyzing whether diffusion limitations successfully describe the results. The dendrimer is modeled as a perfect sphere with the binding sites evenly distributed through shells as a function of the dendrimer's radial direction. The rate of entry of

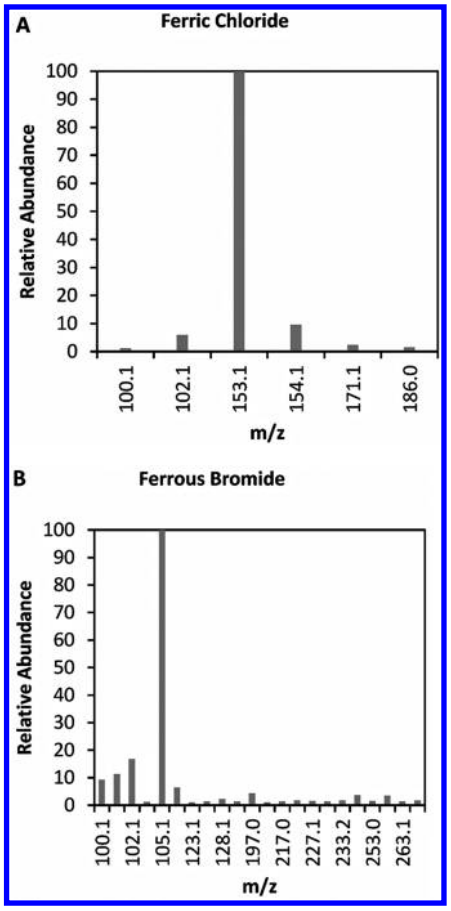

Figure 5. Mass spectra of (A) aqueous ferric chloride−dendrimer mixture at 5 min after LC−MS injection and (B) aqueous ferrous bromide−dendrimer mixture at 2.8 min after LC−MS injection.

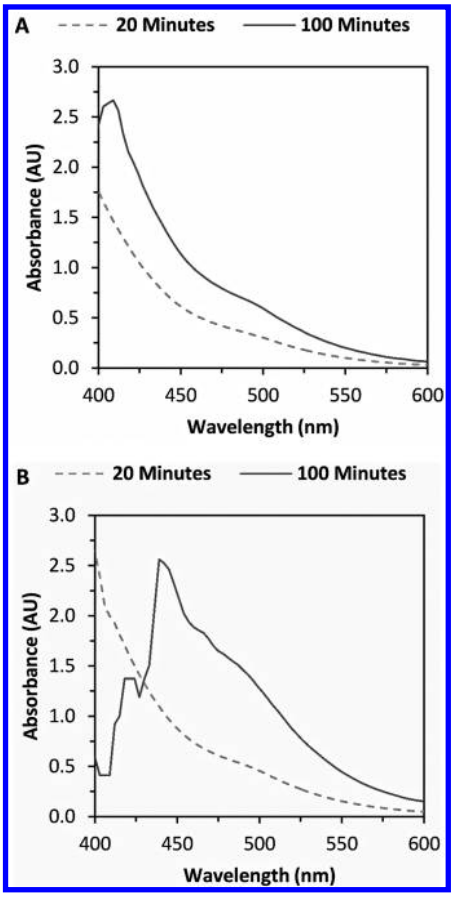

Figure 6. LMCT band of Fe III−dendrimer at (A) T = 22 °C and (B) T = 37 °C at various times after mixing.

metal ions into this sphere (W) is defined as a product of the molar flux (N_A) and the surface area ($4\pi R^2$). In this case, the rate of entry is diffusion-limited.

$$W = 4\pi R^2 N_A = -D\frac{dC}{dr} \quad (3)$$

D, here, represents the diffusion coefficient of metal ions in solution adjusted for counterbalanced halide anions. The initial mass of ions in the solution can be identified as the product of the initial concentration and the volume. The mass at any other time would be determined by integrating the above equation for rate of entry.

$$m_0 = C_0 V \quad (4)$$

$$m(t) = \int_0^t W\, dt \quad (5)$$

These equations can be combined to give us a mass profile that is a function of diffusivity.[29]

$$\frac{m(t)}{m_0} = \frac{6}{\pi^2}\sum_{n=1}^{\infty}\frac{1}{n^2}e^{-Dn^2\pi t/R^2} \quad (6)$$

This model is applied to the concentration profile of ferric chloride for the first 80 min after dendrimer addition. On the basis of the literature,[3,30] a radius of 2.25 nm is used. A diffusivity constant of 2.33×10^{-18} cm^2/s at T = 27 °C is calculated. This value is much smaller than the ion diffusivity of chlorine in water at T = 25 °C of 2.03×10^{-5} cm^2/s calculated by Cussler.[31] Cussler's calculations involve differentiating between the diffusion of the various ions in a compound (such as Na^+ and Cl^- in sodium chloride) when they are solvated in water. The diffusion coefficients of lithium, sodium, and potassium are relatively close in magnitude to chlorine. It is postulated that the aqueous iron compounds involved are in a similar range. Hence, the diffusion coefficient calculated is much too small for the process to be diffusion-limited within the first 80 min of chelation. This result justifies the use of kinetic models for data analysis.

3.3. Rate Law Determination. Ferric chloride of unadjusted pH is used for the rate law determination due to its greater post-chelation solubility. The temperature dependence of the LMCT increase is demonstrated in Figure 6. The effect can be most clearly seen around 460 nm, which is close to the center of the LMCT band. At 460 nm, the absorbance of the spectrum of ferric chloride alone is at its lowest point.

A brief look at the absorbance as a function of time (Figure 7A) reveals a minutely exponential relationship. This effect is observed at every temperature and wavelength within the LMCT band. After about 100 min, the graph becomes almost flat, which suggested the end of the reaction due to chelation of all iron ions. At first glance, it may be tempting to assign a first-order rate law to the reaction. However, when the experiment is repeated using one-half the concentration of ferric chloride but the same concentration of dendrimer, the time for chelation to finish increases by over 4 fold. The same effect is seen when dendrimer

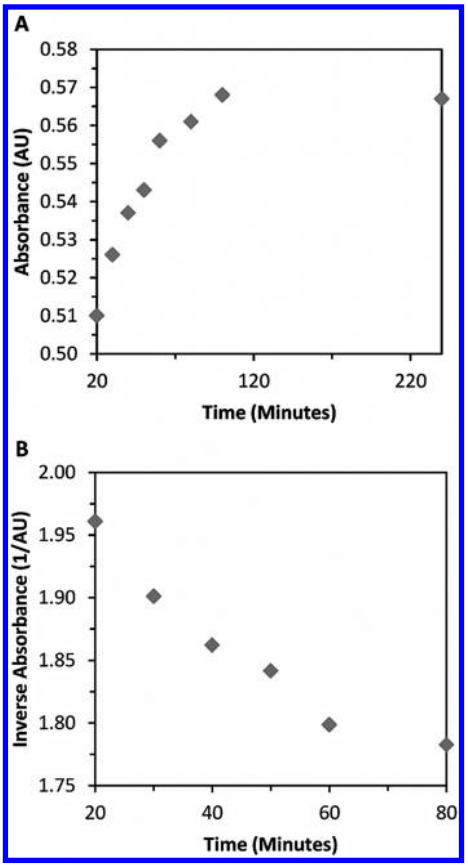

Figure 7. (A) Absorbance at 460 nm as a function of time at $T = 27$ °C and (B) inverse absorbance at 460 nm as a function of time at $T = 27$ °C.

concentration is halved and iron concentration is unchanged. When the concentration of dendrimer is decreased by a factor of 2, the ratio of iron-to-dendrimer reaches 80:1, and, because the dendrimer contains 62 internal amine groups, this ratio could also assist in the drastic reduction in chelation rate.

It is evident, therefore, that both dendrimer and iron concentration effect the rate law. Indeed, the inverse-absorbance, plotted as a function of time (Figure 7B), is also linear, suggesting a second-order rate law.

3.4. Activation Energy Determination. The absorbance as a function of time data is now used to obtain rate constants and an activation energy. The absorbances are first normalized with respect to the absorbance of pure ferric chloride (A_0) and the absorbance obtained upon completion (A_∞).

$$X = \frac{A(t) - A_0}{A_\infty - A_0} \tag{7}$$

X is the fractional conversion, which, for a second-order reaction, can be related to the rate constant linearly.

$$\ln \frac{M - X}{M(1 - X)} = C_0(M - 1)kt \tag{8}$$

M, here, is the stoichiometric ratio of amine binding sites to iron molecules, 62/40. Arrhenius-like behavior can be seen in the comparison of rate constants of different temperatures (Table 1). There is modest variation between the wavelengths, a result of the respective change in molar absorptivity.

Table 1. Rate Constants (L/mol/min) Calculated at Various Temperatures for the Different Wavelengths, Including the Standard Deviations at Each Temperature

temperature (°C)	430 nm	460 nm	490 nm	520 nm	550 nm	580 nm	standard deviation
22	0.026	0.019	0.018	0.018	0.016	0.015	0.004
27	0.031	0.022	0.022	0.021	0.021	0.021	0.004
32	0.034	0.024	0.023	0.022	0.019	0.019	0.006
37	0.075	0.046	0.046	0.044	0.039	0.034	0.014

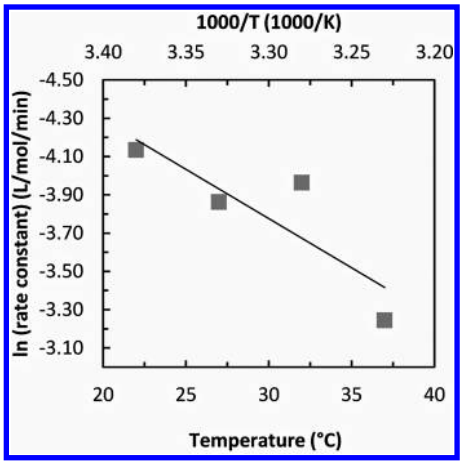

Figure 8. Arrhenius plot of rate constant (calculated from absorbance at 550 nm) as a function of temperature. Results indicate an activation energy of 41.5 kJ/mol.

When applying a linear fit to the Arrhenius plot (Figure 8), activation energies within the order of magnitude of 10 000 J/mol are calculated. The activation energy varies moderately with wavelength, being higher at the start and end of the LMCT band.

The average activation energy between six wavelengths (from 430 to 580 nm) within the LMCT band is 41.5 kJ/mol with a standard deviation of 5.0 kJ/mol. Yamomoto et al.[17] had done a similar experiment using K_2PtCl_4 in which the chelation takes up to 10 days with most happening within the first 18 h. If a similar calculation is performed on this Pt data, an activation energy of 39.4 kJ/mol is found. Because of the similarities between iron and platinum, it is expected that activation energies be relatively close. However, it is understood that the difference in pH and in solvation properties would cause some deviation between the two.

CONCLUSION

Addition of G4-OH dendrimer to aqueous ferric chloride and ferrous bromide is characterized by a slow, steady charge-transfer between the lone pair of electrons on the amine group and the iron acceptor. In both cases, the iron chosen for chelation is dehalogenated and either hydroxylated or hydrated. The chelation of iron is best modeled as a second-order reaction, dependent on the concentrations of both the metal and the dendrimer. The activation energy is approximately 41.5 kJ/mol with a standard deviation of 5.0 kJ/mol.

AUTHOR INFORMATION

Corresponding Author
*Phone: (813) 974-6498. E-mail: jnkuhn@usf.edu.

ACKNOWLEDGMENT

We gratefully acknowledge funding from King Abdulaziz University and start-up funding from the University of South Florida. We thank the Florida Center of Excellence for Drug Discovery and Innovation and Mr. Leigh West. We give thanks to Daigo Yamomoto for providing Pt−dendrimer complexation data and to Prof. Richard Crooks for advice on preparing dendrimers for NMR.

REFERENCES

(1) Tomalia, D. A.; Naylor, A. M.; Goddard, W. A., III. *Angew. Chem., Int Ed. Engl.* **1990**, *29*, 138–175.
(2) Huang, W.; Kuhn, J. N.; Tsung, C.; Zhang, Y.; Habas, S. E.; Yang, P.; Somorjai, G. A. *Nano Lett.* **2008**, *8*, 2027–34.
(3) Scott, R. W. J.; Wilson, O. M.; Crooks, R. M. *J. Phys. Chem. B* **2005**, *109*, 692–704.
(4) Mecke, A.; Lee, I.; Baker, J. R., Jr.; Banaszak Holl, M. M.; Orr, B. G. *Eur. Phys. J. E* **2004**, *14*, 7–16.
(5) Astruc, D.; Chardac, F. *Chem. Rev.* **2001**, *101*, 2991–3024.
(6) Boas, U.; Heegaard, P. M. H. *Chem. Soc. Rev.* **2004**, *33*, 43–63.
(7) Lard, M.; Kim, S. H.; Lin, S.; Bhattacharya, P.; Ke, P. C.; Lamm, M. H. *Phys. Chem. Chem. Phys.* **2010**, *12*, 9285–9291.
(8) Kitchens, K. M.; Ghandehari, H.; Villiers, M. M.; Aramwit, P.; Kwon, G. S. *Nanotechnology in Drug Delivery*; Springer: New York, 2009; Vol. 10, pp 423−59.
(9) Mintzer, M. A.; Grinstaff, M. W. *Chem. Soc. Rev.* **2011**, *40*, 173–190.
(10) Myers, V. S.; Weir, M. G.; Carino, E. V.; Yancey, D. F.; Pande, S.; Crooks, R. M. *Chem. Sci.* **2011**, *2*, 1632–46.
(11) Perez, L. R.; Franz, K. J. *Dalton Trans.* **2010**, *39*, 2177–87.
(12) Gambari, R.; Fibach, E. *Curr. Med. Chem.* **2007**, *14*, 199–212.
(13) Steinberg, M. H. *TheScientificWorldJournal* **2008**, *8*, 1295–1324.
(14) Diallo, M. S.; Balogh, L.; Shafagati, A.; Johnson, J. H., Jr.; Goddard, W. A., III; Tomalia, D. *Environ. Sci. Technol.* **1999**, *33*, 820–24.
(15) Grabchev, I.; Chovelon, J.; Petkov, C. *Spectrochim. Acta, Part A* **2008**, *69*, 100–04.
(16) Labieniec, M.; Watala, C. *Cent. Eur. J. Biol.* **2009**, *4*, 434–51.
(17) Yamamoto, D.; Watanabe, S.; Miyahara, M. T. *Langmuir* **2010**, *26*, 2339–2345.
(18) Yamamoto, D.; Watanabe, S.; Miyahara, M. T. *Ind. Eng. Chem. Res.* **2011**, *50*, 7332–37.
(19) Maiti, P.; Cagin, T.; Lin, S.; Goddard, W., III. *Macromolecules* **2005**, *38*, 979–91.
(20) Sun, L.; Crooks, R. M. *J. Phys. Chem. B* **2002**, *106*, 5864–72.
(21) Van Duijvenbode, R. C.; Borkovec, M.; Koper, G. J. M. *Polymer* **1998**, *39*, 2657–64.
(22) Diallo, M. S.; Christie, S.; Swaminathan, P.; Balogh, L.; Shi, X.; Um, W.; Papelis, C.; Goddard, W. A., III; Johnson, J. H., Jr. *Langmuir* **2004**, *20*, 2640–51.
(23) Niu, Y.; Sun, L.; Crooks, R. M. *Macromolecules* **2004**, *36*, 5725–31.
(24) Chung, Y.; Rhee, H. *Catal. Surv. Asia* **2004**, *8*, 211–23.
(25) Gomez, M. V.; Guerra, J.; Velders, A. H.; Crooks, R. M. *J. Am. Chem. Soc.* **2009**, *131*, 341–50.
(26) Ooe, M.; Murata, M.; Mizugaki, T.; Ebitani, K.; Kaneda, K. *Nano Lett.* **2002**, *2*, 999–1002.
(27) Paiva-Martins, F.; Gordon, M. H. *J. Agric. Food. Chem.* **2005**, *53*, 2704–09.
(28) Taube, H. *Chem. Rev.* **1952**, *50*, 69–126.
(29) Welty, J. R.; Wicks, C. E.; Wilson, R. E.; Rorrer, G. *Fundamentals of Momentum, Heat, and Mass Transfer*, 4th ed.; John Wiley & Sons, Inc.: New York, 2001; pp 531−540.
(30) Li, H.; Zheng, Z.; Cao, M.; Cao, R. *Microporous Mesoporous Mater.* **2010**, *136*, 42–49.
(31) Cussler, E. L. *Diffusion: Mass Transfer in Fluid Systems*, 2nd ed.; Cambridge University Press: New York, 1997; p 143.